UNIVERSITÀ POLITECNICA DELLE MARCHE
Repository ISTITUZIONALE

Push-and-release tests of a steel building with hybrid base isolation

This is the peer reviewd version of the followng article:

Original
Push-and-release tests of a steel building with hybrid base isolation / Dall'Asta, A.; Leoni, G.; Gioiella, L.; Micozzi, F.; Ragni, L.; Morici, M.; Scozzese, F.; Zona, A.. - In: ENGINEERING STRUCTURES. - ISSN 0141-0296. - 272:(2022). [10.1016/j.engstruct.2022.114971]

Availability:
This version is available at: 11566/308521 since: 2024-04-27T17:07:09Z

Publisher:

Published
DOI:10.1016/j.engstruct.2022.114971

Terms of use:

The terms and conditions for the reuse of this version of the manuscript are specified in the publishing policy. The use of copyrighted works requires the consent of the rights' holder (author or publisher). Works made available under a Creative Commons license or a Publisher's custom-made license can be used according to the terms and conditions contained therein. See editor's website for further information and terms and conditions.
This item was downloaded from IRIS Università Politecnica delle Marche (https://iris.univpm.it). When citing, please refer to the published version.

(Article begins on next page)

03 May 2026

Push-and-release tests of a steel building with hybrid base isolation

Andrea Dall'Asta[1], Graziano Leoni[1], Laura Gioiella[1], Fabio Micozzi[1], Laura Ragni[2], Michele Morici[1,*], Fabrizio Scozzese[1], Alessandro Zona[1]

[1] School of Architecture and Design, University of Camerino, Italy

[2] Department of Civil and Building Engineering and Architecture, Università Politecnica delle Marche, Italy

*Corresponding Author: michele.morici@unicam.it

Abstract

Experimental testing of a two-storey 5875 square meters steel braced-frame structure resting on a reinforced concrete slab isolated from the foundations through a hybrid system (28 high-damping rubber bearings and 36 low-friction sliding bearings) is presented. The building incorporates a push-and-release device to evaluate its actual global dynamic response up to displacement amplitudes induced by extreme seismic events, allowing test repetitions during its service life. The testing set up and the experimental campaign, consisting of quasi-static push tests (slow loading and unloading) and push-and-release dynamic tests (slow loading and subsequent sudden release), are described. The experimental results have peculiarities related to the building (structural typology and size, foundation geometry on a steep slope, presence of the push-and-release device for future additional tests), the magnitude of the maximum horizontal displacement never achieved before (285 mm and 227 mm in the quasi-static and dynamic tests, respectively), the global and local monitored parameters (horizontal and vertical displacements, strains, accelerations, in addition to environmental conditions) providing a comprehensive insight into the behaviour of the hybrid isolation system and superstructure.

Keywords: base-isolation, dynamic tests, experimental testing, full-scale tests; push-and-release tests.

1 INTRODUCTION

Base isolation is one of the most effective seismic protection systems for new and existing structures, as proved in more than four decades of studies and applications, e.g., [1]-[13]. Significant changes occurred in the design of base-isolated buildings, form the earliest applications with small design displacements and low design vibration periods (commonly in the range 2.0 to 2.5 s), to more recent solutions with higher values of design displacements and isolation periods. To obtain such large isolation periods, current solutions are oriented towards Curved Concave Surface sliders (CCSs), Lead Rubber Bearings (LRBs), High Damping Rubber Bearings (HDRBs) combined with Low Friction Sliding Bearings (LFSBs) or the use of very large HDRBs [14] which allow reducing the number of the installed isolators. These recent configurations drastically reduced actions transferred to the superstructure, thus, increasing the performance of the base-isolated buildings in terms of service and ultimate limit states. Large displacements associated to high periods can be limited by the damping capacity of the isolation system, which, however, should be not too large to avoid excessive floor accelerations for low intensity events [15].

The structural behaviour of base isolated buildings is strongly influenced by the choices made at the design stage [16] as well as by the actual properties of the bearings and their correct installation. Although both devices and installation were notably improved since the earliest applications, some discrepancies between the design properties and the actual properties of the installed bearings cannot be excluded, also for recent constructions. Such discrepancies deserve much attention in base-isolated structures, where the response is governed by the behaviour of the isolation devices, as they could compromise the seismic performance of the entire building. At this regard, seismic design codes, e.g., [17]-[19], require performing qualification tests and quality production control tests, aimed at evaluating the actual properties of the devices and at demonstrating the compliance with the design requirements. However, a reduced number of

devices is usually tested during quality control, as prescribed by the codes as a function of the device type. For example, the European code [18] prescribes that 20% of HDRBs must be tested while a lower percentage (one device per production lot, constituted by maximum 20 devices) is required for CCSs. Regarding LFSBs, used in hybrid schemes, the European code prescribes the same tests of CCSs only if LFSBs are used to dissipate energy. In the case where devices are used as vertical supports, the conformity to EN 1337 (structural bearings) [20] is only required. Such code does not include tests to verify the low effective friction coefficient of the devices, obtained by using lubricated interfaces. However, the friction coefficients of the adopted devices, as experimentally demonstrated [21], are affected by many parameters and could influence the behaviour of the entire isolation system in the case of a significant number of LFSBs [22].

To overcome these uncertainties and appraise the real behaviour of base-isolated buildings in their as-built condition, testing of the entire building can be made, as documented in [23]-[35] and listed in Table 1. The execution of full-scale tests of the entire building carried out at the end of the construction allows assessing the global behavior of the whole isolation system and the correctness of the device installation, as well as the other components at the interface between the superstructure and substructure, such as seismic gaps. The tests provide a global validation of the dynamic structural performance, which becomes of relevance for strategic constructions. The cost of these full-scale tests is usually marginal if testing planning is incorporated into the building design phase. Moreover, useful information on the behaviour of the superstructure, in addition to information on the isolation system, may be obtained, as documented in [23]-[35].

This article contributes to the existing literature on full-scale push-and-release testing of base-isolated buildings presenting the experimental activities carried out for the new research centre of the University of Camerino, Italy, a two-storey 5875 m^2 steel structure, base-isolated through a hybrid system (28 HDRBs and 36 LFSBs), having 6173 tons of total design mass of

the isolated portion. This isolation system was designed by adopting adequate strategies to provide a high level of robustness and resilience and by considering potential drawbacks related to variability of isolator properties [36][37]. Details on its structural design can be found in [38]. The building incorporates a push-and-release device as well as a permanent structural monitoring system allowing tests to be carried out during the service life of the building to monitor the isolation system behaviour. A short video introducing the building characteristics and showing selected moments of the tests can be found in the YouTube channel of the University of Camerino [39].

In this article, after presenting the testing setup, quasi-static push tests (consisting of slow loading and unloading phases) as well as push-and-release dynamic tests (consisting of a slow loading phase and a subsequent sudden release at an assigned maximum displacement) are illustrated. The results are discussed pointing out some important aspects, i.e., the breakaway force, the behaviour of HDRBs and LFSBs, the residual displacements of the hybrid isolation system, and the superstructure response. It is remarked that the performed tests, that achieved a maximum horizontal displacement never attained before, constitute a reference situation (state zero at construction completed) to be compared to future measurements. These might include recordings during unplanned situations (possible seismic events in an area prone to earthquakes) or planned repetition of the push tests.

2 DESCRIPTION OF THE BUILDING AND TESTING SETUP

2.1 Functions and design objectives of the tested building

The building object of the experimental testing presented in this article is a new research centre of the University of Camerino, called Chemistry Interdisciplinary Project (CHIP), a strategic building hosting high-risk activities and very sensitive instruments of the chemistry and physics laboratories. Its construction was funded by the Italian Department of Civil Protection

(DPC) after the 2016-2017 Central Italy seismic sequence that severely damaged many of the facilities of the University of Camerino. The CHIP building is also intended to work as coordination centre of the DPC during post-earthquake emergency phase in the case of future seismic events. In fact, the town of Camerino, located in the Apennines mountainous part of the Marche region, central-eastern Italy, is one of the most important cultural towns of this seismic-prone area and constitutes a strategic point to observe earthquakes and their effects. Due to its destination, the CHIP building was designed to ensure a structural solution able to guarantee a high level of safety with respect to seismic actions, and at the same time, to permit high construction speed meeting the needs of post-earthquake recovery. Details on the design of the CHIP building and the analyses made for its validation are available in [38]. Construction works began in July 2019, structures were completed in June 2020, the tests here described were made in July 2020, the building inauguration took place in July 2021. Figure 1 shows views of the building during tests (structures completed) and at the inauguration day.

2.2 Superstructure and substructure

The superstructure is a steel braced frame with pinned joints, designed using a 7.2 m × 7.2 m modular system, for a total of 7 modules along each direction, plus a cantilever zone spanning 1.9 m along the entire perimeter of the building (Figure 2), hence, floors are 54.20 m × 54.20 m. Four concentric inverted-V braces were adopted along each principal direction. The steel elements were optimized in terms of dimensions and connection systems based on the single module, resulting in a significant savings on materials and construction time.

The substructure was designed to adapt to the morphology of the area characterized by a remarkable slope, resulting in reinforced concrete (RC) foundations with a complex yet regular geometry and RC rigid columns connecting the deeper foundation levels to the isolation level. The characteristics of the soil and the variability of the thickness of the deformable layer led to the adoption of deep foundations.

2.3 Isolation system

The isolation system consists of 28 HDRBs arranged on the perimeter to maximize torsional stiffness, and 36 LFSBs in the central part to support the higher vertical loads (Figure 3). It was designed assuming an isolation period equal to T_{is} = 3.60 s, able to guarantee a high level of resilience to the building, i.e., the absence of damage on the superstructure and its content up to the maximum design action. In details, HDRBs have diameter 600 mm, total height of rubber 184 mm, horizontal rigidity 0.62 kN/mm and maximum displacement 350 mm (corresponding to a shear deformation of about 200%). This displacement capacity is slightly larger than the displacement demand required at the Collapse Limit State (CLS), return period R_P = 1950 years, which is 324 mm with torsional effects included. In their design, a damping ratio equal to 10% and a shear stiffness equal to 0.4 MPa (soft rubber) were assumed. LFSBs (270 mm of sliding PTFE dimpled disc diameter) have a slightly larger displacement capacity equal to 400 mm and a dynamic friction coefficient lower than 1% at the seismic vertical force condition, as required in the design phase to reduce the sliding force and possible activation of superior modes. The higher value of displacement capacity for the LFSBs is related to their brittle behaviour (loss of support for larger displacements) while HDRBs are supposed to be able to sustain a larger displacement demand (shear deformations more than 200%). Type tests and factory production tests carried out before and after the devices production confirmed the design assumption, except for the damping ratio (14.33%).

2.4 Push-and-release device

The push-and-release testing was foreseen in the design stage of the building to verify the actual behaviour of the isolation system and possible future changes. Hence, a mechanical device for the application of displacements and relevant contrasting structures were designed together with the building. The mechanical device used to apply the target displacement to the base floor of the building consists of an articulated steel structure (Figure 4).

Two hydraulic jacks (with maximum stroke of 300 mm and maximum force of 5000 kN each for a 10 MN of total maximum force) were arranged in series with the mechanical device and two load cells were installed at the interface between the building and the device (Figure 4). The device is a quadrilateral articulated steel strut blocked by the central tie and supported by steel wheels on rails to ensure the longitudinal displacement with a negligible friction force. A sacrificial steel rod (fuse element) made of high strength steel is lodged in the middle of the tie element. The strut angle respect to the pushing direction defines the ratio between the pushing force and the tension force applied to the tie. The high accuracy of the release force is ensured by the small plastic deformation of high strength steel used for the fuse and by its shape which ensures a brittle rupture of the rod. When the fuse breaks, the base-isolated building is released and starts to oscillate in free-vibration conditions. A multiple friction dissipative device, such as those used for falling rock protection barrier, is installed in parallel with the tie element. The dissipating mechanism is based on a friction clamp applying a calibrated force (controlled by Belleville washers) to the looped cable [40]. The loop ensures an end-stroke of the rope sliding, preventing the collision of the device with the lateral walls. After the fuse rupture, the elastic energy stored in the device is partially dissipated by the friction dissipative device, avoiding damages to both the cylindrical articulations and the strut elements. To further secure the load cells from possible impacts during the release phase, the releasing device was anchored to the building side using ratchet belts. It is worth to note that both the device mass and friction force are negligible with respect to the building mass and reaction force.

A reaction box consisting of RC walls and founded on nine piles was arranged in the uphill part of the building to accommodate the testing device. The reinforcements of the building slab, where the releasing device is attached, were detailed according to a strut-and-tie model; punching reinforcements were also added in the RC walls, at the location of the hydraulic jacks.

The push-and-release device may be used to repeat the tests throughout the building life, e.g., to investigate the effect of aging on the HDRBs. Accordingly, the design of the building included a removable floor serving as cover for the reaction box and consisting in a steel girder simply supported on the lateral walls.

2.5 Monitored response parameters and instrumentation

The monitored response parameters included accelerations, displacements, strains, forces, temperature, and relative humidity (RH).

The building was equipped with sixteen uniaxial piezoelectric accelerometers (twelve high sensitivity PCB 393B31 with 0.5 g peak capacity and four PCB 393A03 with 5 g peak capacity), i.e., five at level 0, four at level 1, four at the roof, to characterise the global building response, and the remaining three sensors close to three isolators to monitor the nearby vibrations and detect possible stick-slip effects (Figure 5). The PCB 393A03 were used as back-up in case the PCB 393B31 would saturate during the sudden release following the fuse rupture. However, such situation was not experienced during testing.

Four linear displacement transducers with mechanical stroke 772 mm (Gefran PC67-750) were installed to monitor horizontal displacements; three at the isolation level and one at level 1 between the floor slab and the retaining wall external to the base isolation (Figure 5). Two contactless inductive distance sensors (Baumer IR30.D18L-11179028) were used to monitor vertical displacements by placing a rectified 15 mm thick steel plate connected to the fixed base as target surface.

350 Ohm strain gauges (HBM CXY31-3/350ZE, T rosettes with 2 measuring grids) in half-bridge configuration were applied to two adjacent steel braces at level 0 and to the corresponding two steel braces at level 1 (Figure 5). The choice of the strain gauge with a resistance of 350 Ohm allowed to reduce the influence of the cable resistance in the measurements, while the half-bridge configuration compensates for the effect of temperature.

The force transmitted by the push-and-release mechanical device to the building was monitored through two load cells (AEP CLS500t, 350 Ohm full bridge based with 5000 kN capacity each) and the movements of the building recorded using high-resolution video cameras. The two hydraulic jacks were realized by FPT Fluid Power Technology and controlled by an electric pump with pressure of 700 bar and 1.8 l/m flow rate.

The acquisition of signals from accelerometers, displacement transducers, strain gauges, and load cells, was made through a National Instrument system (one NI 9178 cDAQ equipped with four NI 9234, two NI 9209, and two NI 9237) connected to a laptop running the NI LabView software. Sampling rate was 2048 Hz for accelerometers, load cells, and strain gauges, 100 Hz for displacement traducers. High-quality heavy-shielded cables were employed to connect the sensors to the acquisition system. The environmental conditions, i.e., temperature and RH, were recorded through three standalone digital sensors located at the East corner (EC) and South corner (SC) near the isolators and in the East brace (EB) at level 0 above the isolation, as indicated in Figure 5.

3 EXPERIMENTAL RESULTS

3.1 Performed tests

The experimental tests were performed when the structures were completed, i.e., building without partitions, external walls, architectural elements, and equipment. The total estimated mass of the structures above the isolators during tests was 4633 tons, lower than the design mass (6173 tons) given the absence of live and non-structural dead loads. The total vertical force (45400 kN) was shared as 16600 kN on the 28 HDRBs (mean value of about 600 kN on each HDRB) and 28800 kN on the 36 LFSBs (mean value of 800 kN on each LFSB).

Quasi-static (S) tests, i.e., loading and unloading without sudden release, dynamic (D) tests, i.e., loading up to the rupture of the fuse followed by a sudden release, as well as ambient

vibration recordings (A) were performed on the 3rd and 6th of July 2020. The sequence of the tests is reported in Table 2, with indication of the starting time, the duration of the loading phase for quasi-static and dynamic tests or the duration of the recording interval for ambient vibration tests. The maximum horizontal forces and displacements are also reported, as well as the absolute residual displacement (with respect to the initial condition before the first test) when each test started and 30 minutes after the release in the dynamic tests or 30 minutes after the starting of unloading phase in the static tests. The amplitude of displacements ranged from 109.4 mm to 284.6 mm, being the higher value close to the maximum displacement of the isolation system expected at the CLS. Exception is the first test (S1) where no displacements were recorded as the applied horizontal force was lower than the breakaway friction force, as expected. Regarding the recorded environmental conditions during tests, variations were small at the isolation level (2 to 4 Celsius degrees, 10% in RH) while larger variations (almost 6 Celsius degrees, 20% in RH) were observed in the superstructure.

3.2 Results and discussion

3.2.1. Horizontal displacements

The displacement time-histories recorded during both dynamic and static tests are reported in Figure 6. In the dynamic tests, the time was set to zero when the load cells recorded the drop of the applied horizontal force due to collapse of the fuse. In the quasi-static tests, the time was set to zero when the displacement decrement started. Transducers T1 and T3 monitoring the horizontal displacements in the testing direction (Figure 5) gave the same synchronized readings during both the push and release phases, thus, indicating absence of rotations with respect to the vertical axis. Transducer T2 monitoring the displacement perpendicular to the testing direction confirmed that no transverse movement was activated. Transducer T4 monitoring the horizontal displacements in the testing direction at level 1 gave readings basically superimposed

to that of T1, hence, indicating a rigid-body motion of the building with negligible inter-storey drift, as expected. Test S1 is not included in Figure 6 given that no displacements were initiated, being the applied horizontal force below the breakaway friction force, as already mentioned.

Figure 7 provides a close-up of the displacement time-histories of the dynamic tests, narrowing the time scale in the range of 2 seconds before time zero and 10 seconds after that, to show the dynamic response of the building more clearly after release, highlighting a rapid decay of the oscillatory motion. The time elapsed from the release instant to the second inversion point is variable, ranging between 2,50 s and 3.12 s, thus, the oscillation periods are shorter than the design period (T_{is} = 3.60 s). Different elements contribute to this shift of the isolation period: i) the test mass is lower than the design mass (4633 tons instead of 6173 tons), this alone reduces the isolation period from 3.60 s to 3.25 s; ii) the response concerns a strongly nonstationary motion whose strain energy is rapidly decaying, and the material stiffness is notably nonlinear, with the average stiffness during the initial part of the motion (used to evaluate the equivalent period) notably higher than the average stiffness of a regular oscillation with the same maximum deformation; iii) the concept of isolation period itself in the case of non-stationary conditions (only one oscillation) is somehow an oversimplification of the dynamic response. Indeed, a slightly stiffer response can be observed in the dynamic tests that reached lower displacement levels, e.g., tests D2 and D4 with respect to test D3. This is in accordance with the nonlinear response of the isolation system, whose stiffness increases when the displacement amplitude decreases. Differences can be also observed between tests D1 and D3 because D1 was the first one to deform the virgin rubber in the isolators, accordingly a stiffer response is obtained due to the Mullin's effect of HDRBs [41]-[44] as well as for the lubrication process of the LFSBs [21].

Regarding the residual displacements, two different phenomena contribute to the final behaviour of the isolation system, namely the rate-dependent behaviour with long relaxation time

of the rubber [41] and the friction force of the sliders. The first induces a very different behaviour in quasi-static and dynamic response, as also confirmed by the laboratory tests on HDRB [45]. During the slow loading path, indeed, almost only the elastic component of the rubber is activated, while during the fast release phase viscous over-stresses rise opposite to the elastic response (and so opposite to the recentring force). Consequently, the equilibrium condition reached immediately after the release is not stable as the residual elastic force continue to re-centre the building, while the viscous over-stresses fade away. The final residual displacement at long time is therefore associated to the equilibrium condition between the elastic response of the HDRBs and the friction force exerted by the LFSBs, when over-stresses are completely exhausted. For example, at the end of the oscillatory motion of test D1 an instantaneous residual displacement of around 40 mm was observed (Figure 7), then it decreased to 15.7 mm after 30 minutes and to 15.2 mm before the subsequent tests (S2), as reported in Table 2. After the static test S2, the residual displacement was 26.1 mm that reduced to 22.1 mm after 3 days of rest. The amplitude of the residual displacement in the following dynamic tests D2, D3, and D4 was always in the range 22 to 23 mm. Only in the last test (S3), where the maximum displacement was imposed, the residual displacement was higher and equal to 36.2 mm 30 minutes after the initiation of the unloading phase (as indicated in Table 2) and 32.2 mm after one hour. The recovery of the residual displacement, due to the viscous behaviour of the HDRBs, continued and after one month a final residual displacement equal to 25 mm was measured, in accordance with the expected friction force exerted by the sliders. Further considerations on the friction force are discussed in the following paragraph, based on load cell measures. The damping properties of the isolation system cannot be directly deduced from observed motions using the common exponential decay law because of the long-term viscous response of the rubber that strongly affects the release free vibration phase (the system oscillates without crossing the 0 displacement, see Figure 7), as previously described. Equivalent stiffness and damping of this

system can be deduced only developing more detailed studies including adequate rubber models [41] that are beyond the objectives of this paper.

It is remarked that this level of details in the experimental horizontal displacement response for a full-scale hybrid base isolation system engaged up to displacements of this amplitude (expected at the CLS) is not available in other push-and-release tests appeared to date in the technical literature (Table 1). This represents a unique contribution of this study, giving important validations of structural behavioural aspects of hybrid base isolation that were in the past object of numerical simulations or experimental tests involving isolators only, as smaller amplitudes of horizontal displacements were attained in other full-scale tests, as already commented.

3.2.2. Forces

Figure 8 illustrates the horizontal force-displacement curves in the loading phase up to the release for the dynamic tests as well as the horizontal force-displacement curves in the loading and unloading phases for the static tests. Moreover, the release point for the dynamic tests is highlighted by a dot. After that, only for the dynamic tests, the unloading branch of the hysteresis loop were estimated multiplying the accelerations derived from the displacements and the overall isolated mass, i.e., computing the inertial forces that, according to the dynamic equilibrium, are equal to the sum of the recentring and dissipating contributions. In test D1 the structure was moved for the first time from its initial position and a breakaway friction force equal to 700 kN is reached (resulting in a breakaway friction coefficient of 2.4%). In the subsequent tests, smaller values of the breakaway friction force were found. Such a reduction can be explained considering that the trajectory followed in all the tests is the same, thus, the lubrication of the sliding surfaces increased test after test, in accordance with phenomena already observed [21]. Moreover, it should be remarked that the building did not start from the initial position in the tests following D1 and, accordingly, the initial force measured to start the movement was

not only related to the friction of LFSBs but also to the residual force of HDRBs. The test D1 is also influenced by the first cycle effect of the virgin rubber, i.e., the first time that the HDRBs reach this level of strain [41]-[44], as already commented. Such a different behaviour of the virgin rubber is clearly observed in Figure 8 where all the tests have a substantially overlapping loading path except for D1. The unloading branches calculated for the dynamic tests from the accelerations are different compared to those of the static tests (S2 and S3) because of the different velocity involved: in the dynamic test the viscous component of the rubber strongly increase the energy dissipated whereas during static tests, this viscous component is not significant (as also showed later in Figure 10).

The response observed in the static tests S2 and S3 (Figure 8) is typical of hybrid isolation systems, where, in addition to the response of HDRBs, a small friction component due to LFSBs can be observed [26][29]. An initial friction force as well as a drop of the force at the inversion point of the displacement (equal to twice the friction force) can be noted. A close-up at the inversion of tests S2 and S3 is reported in Figure 9: the vertical drop at the beginning of the back displacement (measured after the small viscous relaxation of the rubber due to a not instantaneous displacement inversion) is around 400 kN (500 kN for S2 and 300 kN for S3), resulting in a friction coefficient of 1.4% (1.7% for S2 and 0.1% for S3). Consequently, the total dynamic friction force of the sliders (at low velocity) can be estimated equal to $F_s = 200$ kN. By considering that the total weight force acting on the sliders is 28800 kN the corresponding dynamic friction coefficient at slow velocity (quasi-static test) is 0.7%, in accordance with the design prescription (friction coefficient less than 1%). The breakaway friction coefficient is instead larger, i.e., 2.4%, based on the breakaway friction force observed in test D1. It is worth to recall that the friction coefficient also depends on the vertical pressure that is lower than the design seismic condition, i.e., the mass during the in-field tests was lower than the one during service condition (during tests the mean stress on the sliding PTFE dimpled disc was 14 MPa while the mean design stress is 43 MPa). Since the friction coefficient decreases by increasing

the vertical load, the friction coefficient will be even lower in the design condition (at the end of the building construction when non-structural dead loads as well as live loads are added).

Figure 10 shows the loading ramp of the tests with largest displacements (S2, D3 and S3), once deducted of the dynamic friction force (200 kN) previously estimated and scaled with respect to a single HDRB, i.e., divided by the numbers of HDRBs. This allows to compare the obtained experimental curves with the control tests carried out on some isolators before their installation. Specifically, the loading ramp of the One Side Ramp (OSR) test and the third cycle of the Horizontal Cyclic Characteristic (HCC) test at 150% of shear deformation are reported. It is observed the full agreement between the experimental curves and the OSR test (both in the quasi-static range of load velocity), confirming the correctness of the global stiffness of the HDRBs and the negligible viscous over-stresses generated by the rubber in this range of velocities. On the contrary, in the dynamic range of velocity the viscous behaviour of this kind of rubber leads to a significant strain-rate dependent behaviour as shown by the HCC test (performed in laboratory at 0.5 Hz, with a mean speed of 550 mm/s).

It is again highlighted the contribution of this study, where the level of details in the experimental measure of forces in a full-scale hybrid base isolation system engaged up to displacements expected at the CLS, not found in previous publications, is an important contribution to provide data for the assessment of research on isolator models.

3.2.3. Vertical displacements

Figure 11 reports the vertical displacement measurements versus the horizontal displacement measurements of both the monitored HDRB and the monitored LFSB, i.e., inductive sensors V2 and V1 and the displacement transducer T1 in Figure 5. It can be observed that vertical displacements are very small even during the tests with largest horizontal displacements, confirming the full compatibility of the HDRBs with the LFSBs in the hybrid isolation system. In fact, the vertical displacements of the latter, also monitored by the inductive sensor V1, were

substantially zero during all the test series, with an initial cyclic behaviour recorded during the test S2 mainly related to a regularization of the lubricated sliding surface.

It is worth stressing another original element of this current experimental activity, i.e., the analysis of the vertical displacement in a full-scale hybrid base isolation system pushed up to such high displacements (consistent with CLS), which could reveal useful to assess the compatibility of HDRBs and LFSBs in terms of vertical deformations.

3.2.4. Brace strains

With regard to the superstructure response, the strains measured in the braces between levels 0 and 1 as well as between levels 1 and 2 (respectively strain gauges G2 and G4 in Figure 5) in the same time interval of Figure 7 are reported in Figure 12 for the dynamic tests D3 and D4. From these deformation histories it can be easily seen both the vibration motion of the isolation system and the higher vibration modes of the superstructure. Moreover, the peak values of 0.07 micro-strain and 0.14 micro-strain (drift of an order of 10^{-4}) confirm the rigid motion of the building above the isolation system, as already commented from the displacement readings. The frequency content of the brace strains in the time window from 0 to 10 s are reported in Figure 13 and Table 3 for tests D2, D3, and D4 (results for test D1 are missing as the strain gauges were not connected to the acquisition unit). Results clearly identify the vibration period of the isolation system as well as the higher frequencies of the super-structure, confirming that the brace strains are a valuable additional source of information, not only for the structural response of the steel superstructures, but for the base isolation system as well.

It is remarked that no other published push-and-release test on a base isolated building provided the experimental recordings of the response of braces in the superstructure. The fact that it is possible to monitor the response of the base isolated building from the strains of its braces, gaining significant insight into its dynamic response, is an interesting achievement of this study, with potential applications in future monitoring installations.

3.2.5. Accelerations

Finally, a selection of the accelerometric recordings is given in Figure 14 (tests D3 and D4). The acceleration peaks recorded during the release phase in D3 at level 0 above isolation at about 0.5 s were a consequence of the whip determined by the fracture of the steel wire rope in the push-and-release device, also documented in the video of the test [39]. Such a fracture only occurred in test D3 and only influenced the readings of the accelerometers in the floor directly connected to the push-and-release device. The accelerations recorded during the dynamic tests are very small, proving that the motion after the sudden release, even in test D3, could be only marginally felt by persons inside the building (as directly testified by the Authors of this article). In particular, the accelerations at the first floor (level 1) and at the roof (level 2) are very similar due to the nearly rigid-body motion, as already commented. The accelerations in the floor connected to the push-and-release device (level 0 above isolation) are slightly larger than those recorded at the upper floors due to dynamic effect of the fuse collapse (its peak is very rapidly damped). The analysis of the frequency contents of the accelerations in the time window from 0 to 10 s is summarized in Figure 15 and Table 3. It is interesting to observe the very good agreement of the peaks in the frequency contents of the signals acquired through accelerometers and strain gauges, despite the accelerometric acquisition system was working at its limit in terms of lower frequency response and frequency resolution (0.1 Hz to highlight the transient response).

Ambient vibration tests, whose results are summarized in Table 4, present very small differences in terms of dominant frequency contents, thus, testifying that no modifications that could affect the dynamic response of the building in terms of modal frequencies of the first three modes occurred during the tests. As expected, the frequency identified during ambient vibration test are always related to the fixed-base configuration of the building, i.e., the LFSBs friction act as rigid connection between the superstructure and substructure horizontal displacement,

and consequently the isolation characteristics cannot be identified using this type of measurements for hybrid system as far as for any kind of friction-based systems [46]. These results will constitute a basis for future comparisons that will be made following operational vibration tests repeated during the service life of the building.

It is noted that ambient vibrations tests were rarely performed during other push-and-release tests published in the technical literature (Table 1). Comparing the ambient vibration tests between push-and-release tests, the dynamic analysis of the structural response after release from accelerometer as well as strain gauges in the braces, constitute a unique contribution of this study, expected to provide useful information for future monitoring applications of base isolated buildings.

4 CONCLUSIONS

This article presented an experimental campaign consisting of quasi-static loading/unloading tests, as well as push-and release dynamic tests on a strategic steel braced frame building isolated at the base through a hybrid system combining HDRBs and LFSBs. Points of interest follow.

- The magnitude of the maximum horizontal displacement achieved in quasi static tests (284.6 mm) and in the dynamic tests (226.9 mm) are much larger than other similar tests documented up to date in the technical literature and they are close to the design displacement used for the isolation system verification. Consequently, the presented tests are a demanding experimental full-scale engagement of the hybrid isolation system and a verification of its installation.
- A comprehensive system of sensors was conceived to collect information on the structural response at local and global level, as well as to recover data for the characterization of low frequency vibrations related to the seismic isolation system and the high frequency vibrations related to the vibration modes of the superstructure.

The sensor system included accelerometers, displacement transducers, strain gauges, load cells, in addition to environmental temperature and humidity sensors.

- The building showed rigid-body motions during the tests with negligible inter-storey drift and no parasitic torsional movements, in accordance with the design objectives.
- Very small floor accelerations were observed, confirming the effectiveness of the designed isolation system in protecting the building structure and contents during strong earthquakes.
- Measured vertical displacements were very small for HDRBs and almost zero for the LFSBs, settling the full compatibility of these two different devices in the hybrid isolation design even for high lateral displacements.
- A notably different response was observed in quasi-static tests (low velocity) and dynamic tests (high velocity) due to the viscoelastic behaviour of HDRBs. Consequently, residual displacements are influenced by both the significant rate-dependent behaviour with long relaxation time of the rubber in HDRBs and the friction force of the LFSBs.
- The breakaway force and the friction force can be easily estimated from the static tests.
- Comparison with control tests made on some HDRBs confirmed the correctness of the global stiffness of the HDRBs.

These results will be the object of future further studies, also using the experimental data that will be acquired during repetitions of the push-and-release tests as well as from the response of the building in possible future seismic events that would activate displacements in its isolation system. This last possibility is very important, as this kind of tests, even if pushed up to very high displacements, cannot be directly superimposed to the real dynamic behaviour of the isolated building during an earthquake.

ACKNOWLEDGEMENTS

The financial support for these tests provided by the Italian Department of Civil Protection is gratefully recognized. A special acknowledgement goes to Angelo Borrelli, head of the Italian Department of Civil Protection at the time of this project. The authors recognise the indispensable support from colleagues and collaborators at the University of Camerino, namely Gian Luca Marucci, Cristiano Bordo, and Irene Pisani for technical and logistic assistance, Raniero Carloni, Luca Montecchiari, and Andrea Orlando for video documentation, Egizia Marzocco for communication coordination, Claudia Canuti, Nicola Ceccolini, and Leonardo Cipriani for providing support in the structural monitoring operations. Finally, the authors are grateful to Claudio Pettinari, Rector of the University of Camerino, for strongly promoting this project.

REFERENCES

[1] Kelly JM. Aseismic base isolation: review and bibliography. *Soil Dynamics and Earthquake Engineering*. 1986;5(4):202-216.

[2] Kelly JM, Aiken ID. Experimental studies of the seismic response of structures incorporating base-isolation systems. *Nuclear Engineering and Design*. 1991;127(3):329-338.

[3] Stewart JP, Conte JP, Aiken ID. Observed behavior of seismically isolated buildings. *Journal of Structural Engineering*. 1999;125(9):955-964.

[4] Nagarajaiah S, Xiaohong S. Response of base-isolated USC hospital building in Northridge earthquake. *Journal of Structural Engineering*. 2000;126(10):1177-1186.

[5] Nagarajaiah S, Sun X. Base-isolated FCC building: Impact response in Northridge earthquake. *Journal of Structural Engineering*. 2001;127(9):1063-1075.

[6] Warn GP, Ryan KL. A review of seismic isolation for buildings: historical development and research needs. *Buildings*. 2012;2(3):300-325.

[7] Makris N. Seismic isolation: Early history. *Earthquake Engineering and Structural Dynamics*. 2019;48(2):269-283.

[8] De Luca A, Guidi LG. State of art in the worldwide evolution of base isolation design. *Soil Dynamics and Earthquake Engineering*. 2019;125(1):105722.

[9] Clemente P, Martelli A. Seismically isolated buildings in Italy: State-of-the-art review and applications. *Soil Dynamics and Earthquake Engineering*. 2019;119(1):471-487.

[10] De Luca A, Guidi LG. Base isolation issues in Italy: Integrated architectural and structural designs. *Soil Dynamics and Earthquake Engineering*. 2020;130(1):105912.

[11] De Domenico D, Tubaldi E, Takewaki I, Karavasilis T, Dall'Asta A, Lavan O. Recent advances and applications of seismic isolation and energy dissipation devices. *Frontiers in Built Environment*. 2020;6(1):126.

[12] Freddi F, Galasso C, Cremen G, Dall'Asta A, Di Sarno L, Giaralis A, Gutiérrez-Urzúa F, Málaga-Chuquitaype C, Mitoulis SA, Petrone C, Sextos A, Sousa L, Tarbali K, Tubaldi E, Wardman J, & Woo G. Innovations in earthquake risk reduction for resilience: Recent advances and challenges. *International Journal of Disaster Risk Reduction* 2021; 60: 102267.

[13] Ragni L, Micozzi F, Tubaldi E, Dall'Asta A. Behaviour of structures isolated by HDNR Bearings at design and service conditions. *Journal of Earthquake Engineering*, 2022;26(4):1743-1766.

[14] Committee of Foreign Affairs, JSSI. *Introduction of the Structural Calculation Method for Seismically-Isolated Building in Japan.* March 2020.

[15] Yang TY, Konstantinidis D, Kelly JM. The influence of isolator hysteresis on equipment performance in seismic isolated buildings. *Earthquake Spectra*. 2010;26(1):275-293.

[16] Micozzi F., Scozzese F., Ragni L., Dall'Asta A. Seismic reliability of base isolated systems: sensitivity to design choices. Engineering Structures. 2022; 256(1):114056

[17] Italian Building Code 2018 (In Italian), Ministry of Infrastructures and Transport, Rome, Italy, 2018.

[18] EN 15129:2009 Antiseismic devices, European Committee for Standardization, Brussels, Belgium, 2009.

[19] ASCE/SEI 7-16. Minimum design loads for buildings and other structures. American Society of Civil Engineers: Structural Engineering Institute, Reston, VA 2017.

[20] EN 1337-1:2000 Structural bearings – Part 1: General design rules, European Committee for Standardization, Brussels, Belgium, 2000.

[21] Dolce M, Cardone D, Croatto F. Frictional behavior of steel-PTFE interfaces for seismic isolation. *Bulletin of Earthquake Engineering*. 2005;3(1):75-99.

[22] Ragni L, Micozzi F, Tubaldi E, Dall'Asta A. Behaviour of structures isolated by HDNR bearings at design and service conditions. *Journal of Earthquake Engineering*, 2020; DOI: 10.1080/13632469.2020.1776792

[23] Giuliani GC. Structural design, analysis and full-scale tests of seismically isolated buildings. *Engineering Structures*. 1993;15(2):102-116.

[24] Bixio AR, Dolce M, Nigro D, Ponzo FC, Braga F, Nicoletti M. Repeatable dynamic release tests on a base-isolated building. *Journal of Earthquake Engineering* 2001;5(3):369-93.

[25] Braga F, Laterza M. Field testing of low-rise base isolated building. *Engineering Structures*, 2004;26(11):1599-1610.

[26] Braga F, Faggella M, Gigliotti R, Laterza M. Nonlinear dynamic response of HDRB and hybrid HDRB-Friction sliders base isolation systems. *Bulletin of Earthquake Engineering*. 2005;3(1):333-353.

[27] Cardone D, Dolce M, Ponzo FC. The behaviour of SMA isolation systems based on a full-scale release test. *Journal of Earthquake Engineering*. 2006;10(1):815-842.

[28] Oliveto G, Marletta M. Seismic retrofitting of reinforced concrete buildings using traditional and innovative techniques. *ISETJ Earthq Technol* 2005;42(2-3):21–46.

[29] Oliveto ND, Scalia G, Oliveto G. Dynamic identification of structural systems with viscous and friction damping. *Journal of Sound and Vibration*. 2008;318(4-5):911-926.

[30] Ponzo FC, Di Tommaso R, Nigro D, Romaniello R, Cardone D. Analysis of dynamic behaviour of a base isolated building: a release test in Augusta (SI). *2nd European conference on earthquake engineering and seismology*, Instanbul, 2014.

[31] Athanasiou A. Dynamic identification of the Augusta hybrid base isolated building using data from full scale push and sudden release tests. Ph.D. Dissertation. Italy: University of Catania; 2015.

[32] Athanasiou A, Oliveto DS, Ponzo FC. Identification of first and second order models for the superstructure of base-isolated buildings using free vibration tests: A case study. *Soil Dynamics and Earthquake Engineering*. 2020;135(1):106178.

[33] Ferrotto MF, Cavaleri L, Di Trapani F, Castaldo P. Full scale tests of the base-isolation system for an emergency hospital, *7th ECCOMAS Thematic Conference COMPDYN 2019*. Crete, Greece.

[34] Wu YX, Dong XJ, Lin YQ, Cheng HD. Field test for a base isolation structure on condition of horizontal and initial displacement. *Applied Sciences*. 2022;12(1):232.

[35] Okumura Corporation. Efforts for the seismic isolation promotion (in Japanese). 2017. https://www.okumuragumi.co.jp/environment/report/2017/pdf/2017_p11-12.pdf

[36] Ragni L, Cardone D., Conte N, Dall'Asta A, Di Cesare A, Flora A, Leccese G, Micozzi F, Ponzo C. Modelling and seismic response analysis of Italian code-conforming base-isolated buildings. *Journal of Earthquake Engineering*. 2018;22(S2):198-230.

[37] Franchin P, Ragni L, Rota M, Zona A. Modelling uncertainties of Italian code-conforming structures for the purpose of seismic response analysis. *Journal of Earthquake Engineering*. 2018;22(S2):28-53.

[38] Dall'Asta A, Leoni G, Micozzi F, Gioiella L, Ragni L. A resilience and robustness oriented design of base-isolated structures: The New Camerino University Research Center. *Fontiers in Built Environment.* 2020;6(1):50.

[39] https://youtu.be/Ou95s6_Jcws

[40] Castanon-Jano L, Blanco-Fernandez E, Castro-Fresno D, Ballester-Muñoz F. Energy dissipating devices in falling rock protection barriers. *Rock Mechanics and Rock Engineering* 2017;50(3):603-619.

[41] Tubaldi E, Ragni L, Dall'Asta A, Ahmadi H, Muhr A. Stress softening behaviour of HDNR bearings: modelling and influence on the seismic response of isolated structures. *Earthquake Engineering and Structural Dynamics.* 2017;46(12):2033-2054.

[42] Quaglini V, Dubini P, Vazzana G. 2015. Experimental Assessment of High Damping Rubber Under Combined Compression and Shear. *J. Eng. Mater. Technol.* 2015;138:011002.

[43] Ragni L, Tubaldi E, Dall'Asta A, Ahmadi H., Muhr A. Biaxial shear behaviour of HDNR with Mullins effect and deformation-induced anisotropy. *Engineering Structures*. 2018;154(1):78-92.

[44] Abe M, Yoshida J, Fujino Y. Multiaxial Behaviors of Laminated Rubber Bearings and Their Modeling. I: Experimental Study. *Journal of Structural Engineering.* 2004;130:1119-1132.

[45] Dall'Asta A, Leoni G, Micozzi F, Gioiella L, Ceccolini N, Ragni L. The new Camerino university research center: design of the base-isolated building and dynamic testing. *8th ECCOMAS Thematic*

Conference on Computational Methods in Structural Dynamics and Earthquake Engineering COMPDYN 2021. Athens, Greece, 27–30 June 2021.

[46] Kelly JM. Earthquake-Resistant Design with Rubber. *Springer London*; 1997. DOI: 10.1007/978-1-4471-0971-6

Table 1: Push-and-release tests documented in the technical literature

Location and references	Isolation	Super-structure	Release device	Tests
Ancona (Italy) [23]	66 HDRBs	Seven-storey 875 m^2 per storey Total mass 6300 tons	Dynamite	Push-and release tests with max displacement 107 mm Pulsating force vibrations
Potenza (Italy) [24]	89 HDRBs arranged at two different levels	Five/six storey 2200 m^2 per storey Total mass 15014 tons	Mechanical (Snap-through mechanism)	Ambient and small amplitude free vibration tests Push and release tests up to 18.8 mm
Rapolla (Italy) [25][26][27]	Three configurations: (a) 28 DRBs (b) 12 HDRBs + 16 LFSBs (c) 28 LFSBs + 3 SMA	Three-storey 500 m^2 per storey Total mass 1000 tons	Mechanical (Snap-through mechanism)	Quasi-static loading and un-loading tests and push-and release tests up to 170 mm (a), 165 mm (b) and 140 mm (c)
Solarino (Italy) [28][29]	12 HDRBs + 13 LFSBs	Four-storey about 200 m^2 per storey Total mass 1237 tons	Mechanical (High-strength steel rod)	Quasi-static loading and unloading tests up to 128 mm Push-and release tests up to139 mm
Augusta (Italy) [30][31][32]	16 HDRBs + 20 LFSBs	Two -storey 571m^2 per storey Total mass 2100 tons	Mechanical (High-strength steel rod)	Push-and release tests up to 116 mm
Palermo (Italy) [33]	41 DFPs	Three-storey about 900 m^2 per storey Total mass 2900 tons	Mechanical (High-strength steel rod)	Quasi-static loading and unloading with max displacement 150.7 mm Push-and release tests with max displacement 121 mm Ambient vibrations
China [34]	20 HDRBs + 26 LRBs	Three-storey 1195 m^2 per storey Total mass 5586 tons	Dynamite	Push-and release tests with max displacement 75 mm Ambient vibrations
Japan [35]	25 LDRBs + 12 dampers	Four-storey 348.18 m^2 per storey Total mass 2500 tons	Mechanical	Push-and release tests with max displacement 100 mm (repeated in 1986, 2005 and 2016)
Camerino (Italy) [this article]	28 HDRBs + 36 LFSBs	Two-storey 2937 m^2 per storey Total mass 4633 tons	Mechanical (High-strength steel rod)	Quasi-static loading and unloading with max displacement 284.6 mm Push-and release tests with max displacement 226.9 mm Ambient vibrations

Table 2: Tests sequence

Day	Test	Starting time	Duration [min]	Max Force [kN]	Max displacement [mm]	Displacement at test start [mm]	Displacement 30 min after release/un-loading start [mm]
3rd July 2020	A1	10:55	30	-	-	-	-
	S1	12:22	6	518	0.0	0.0	0.0
	D1	13:47	16	2729	177.3	0.0	15.7
	S2	16:36	21	3206	232.4	15.2	26.1
6th July 2020	A2	10:11	40	-	-	-	-
	D2	12:24	8	1756	109.4	22.1	22.4
	D3	13:36	18	3122	226.9	22.1	23.4
	A3	15:27	23	-	-	-	-
	D4	15:56	9	1786	121.8	22.1	22.9
	S3	17:07	25	3834	284.6	22.6	36.2

Table 3: Periods and frequencies identified in the dynamic tests (10-second time window after release)

Source	Test	T_1 [s]	f_1 [Hz]	T_2 [s]	f_2 [Hz]	T_3 [s]	f_3 [Hz]
Strain gauges	D1	-	-	-	-	-	-
	D2	2.51	0.40	0.21	4.70	0.11	8.80
	D3	2.51	0.40	0.21	4.70	0.11	8.70
	D4	2.00	0.50	0.21	4.70	0.11	8.80
Accelerometers	D1	2.00	0.50	0.21	4.70	0.11	8.70
	D2	2.15	0.47	0.21	4.80	0.11	8.73
	D3	2.15	0.47	0.21	4.73	0.12	8.67
	D4	2.15	0.47	0.21	4.67	0.11	8.80

Table 4: Periods and frequencies identified in the ambient vibration recordings

Test	T_1 [s]	f_1 [Hz]	T_2 [s]	f_2 [Hz]	T_3 [s]	f_3 [Hz]
A1	0.31	3.28	0.28	3.60	0.25	3.95
A2	0.30	3.29	0.28	3.59	0.26	3.91
A3	0.31	3.28	0.28	3.58	0.26	3.91

(a) North aerial view during tests

(b) South-West aerial view during tests

(c) South-East view of the pushing device box

(d) North-West prospect at inauguration

Figure 1: Views of the CHIP building during the tests (July 2020) and at inauguration (July 2021).

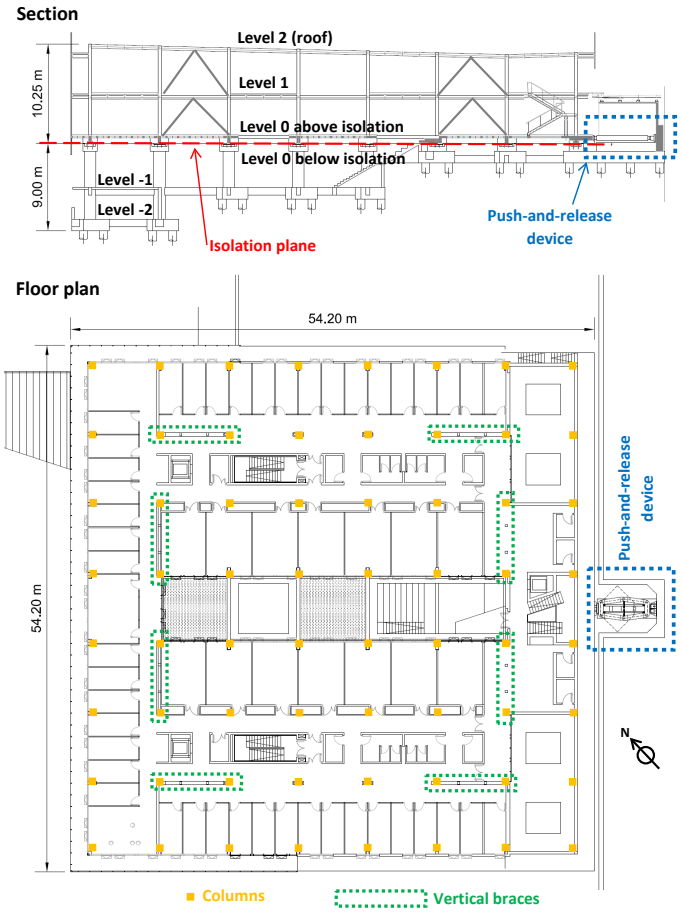

Figure 2: Floor plan and section of the CHIP building.

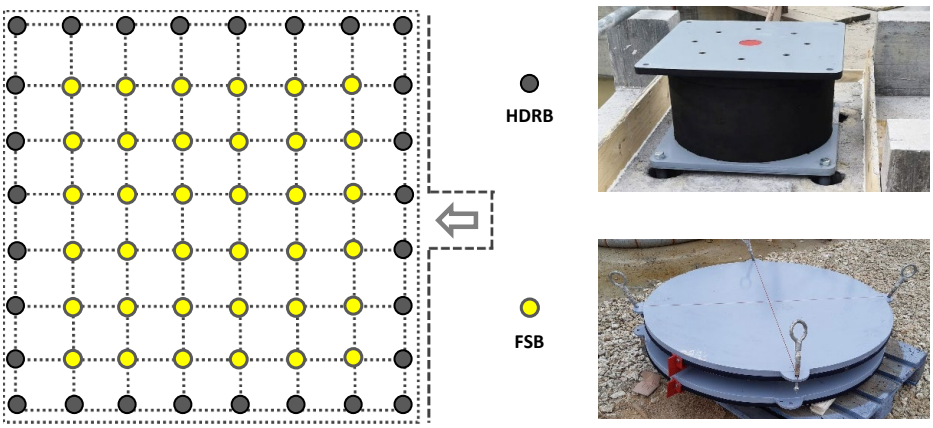

Figure 3: Isolation layout and pictures of the devices.

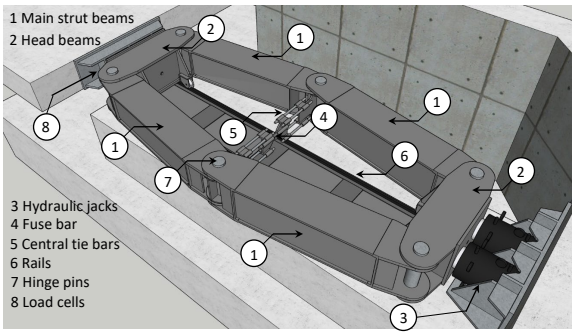

(a) Scheme of the device

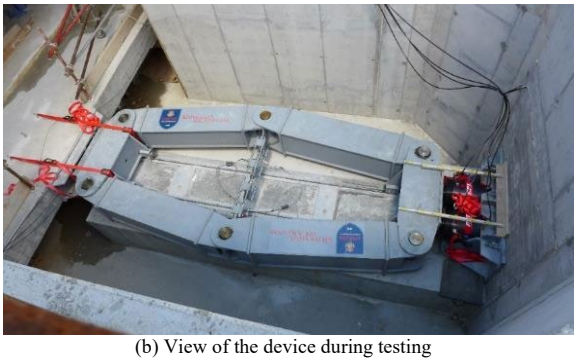

(b) View of the device during testing

(c) View of the central tie bars and fuse bar

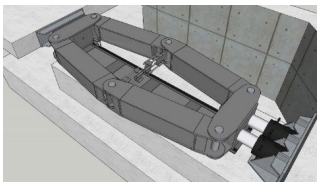

(d) Push phase

(e) Close-up of the fuse bar

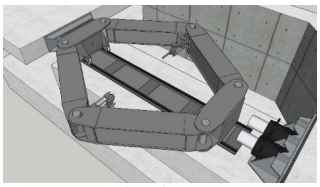

(f) Release

(g) Collapsed fuse bar

(h) Close-up of the friction device

Figure 4: Push-and-release device.

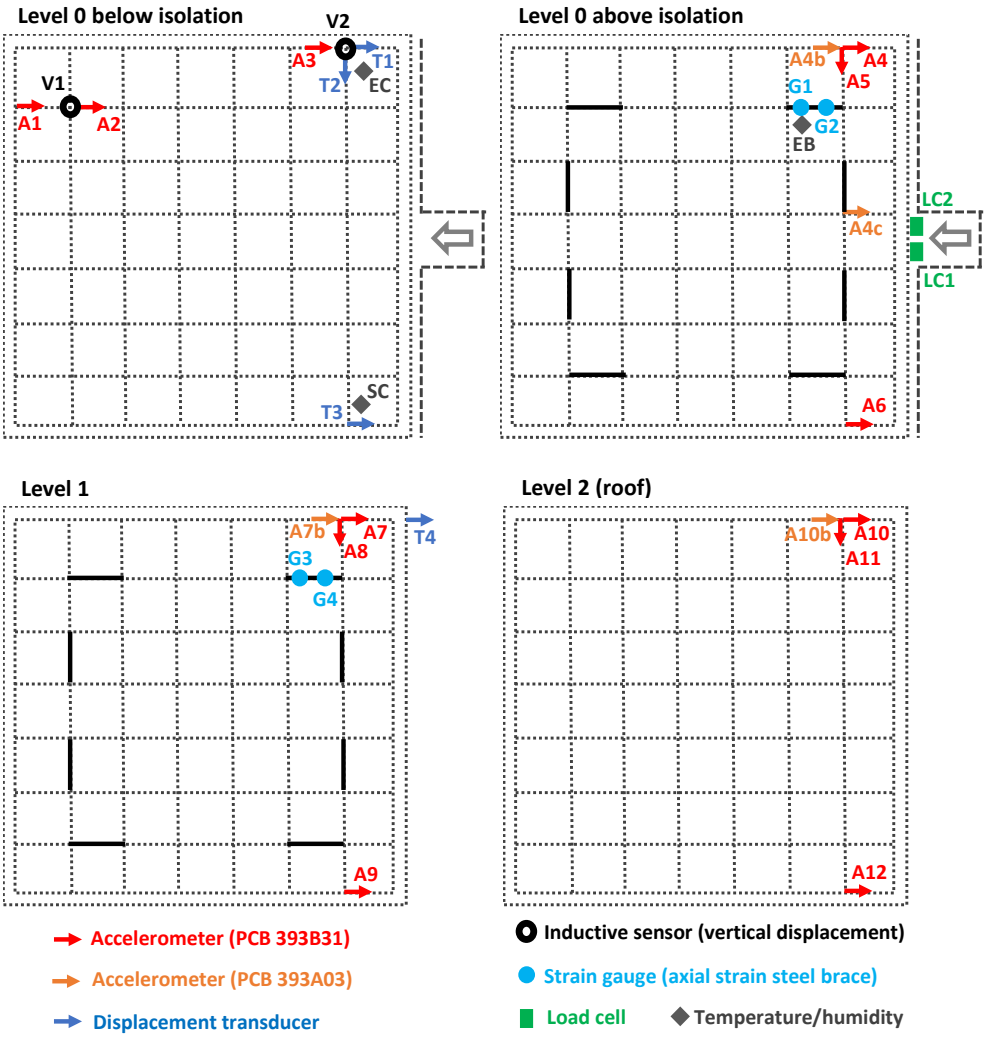

Figure 5: Sensor layout during the tests.

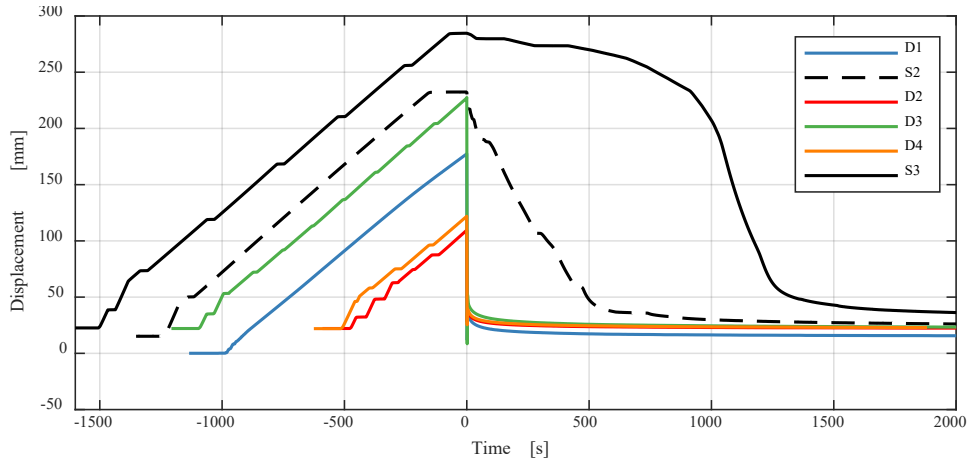

Figure 6: Displacement time-history curves of the dynamic and static tests.

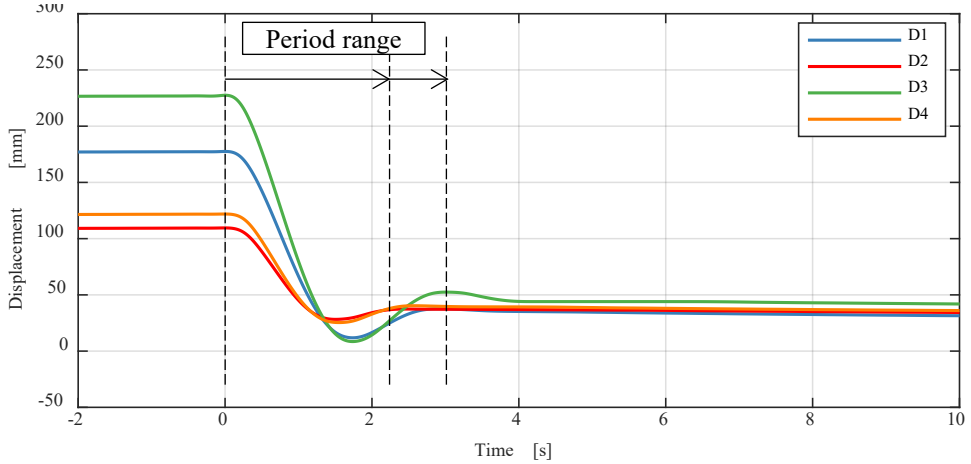

Figure 7: Displacement time-history curves of the dynamic tests (close-up of the release phase).

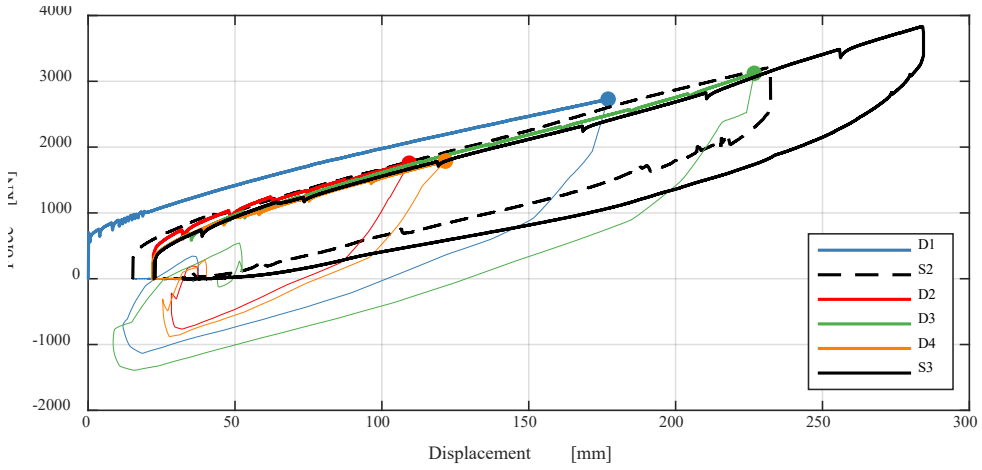

Figure 8: Force-displacement curves of the dynamic and static tests.

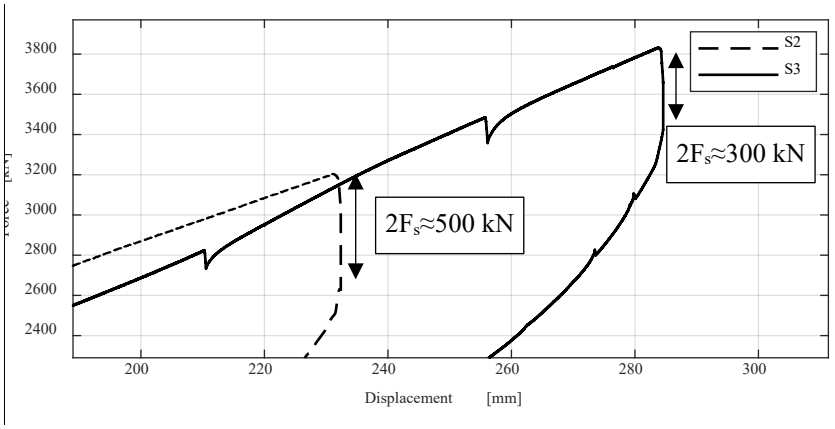

Figure 9: Detail of the force-displacement curves of the tests S2 and S3 at the displacement inversion point.

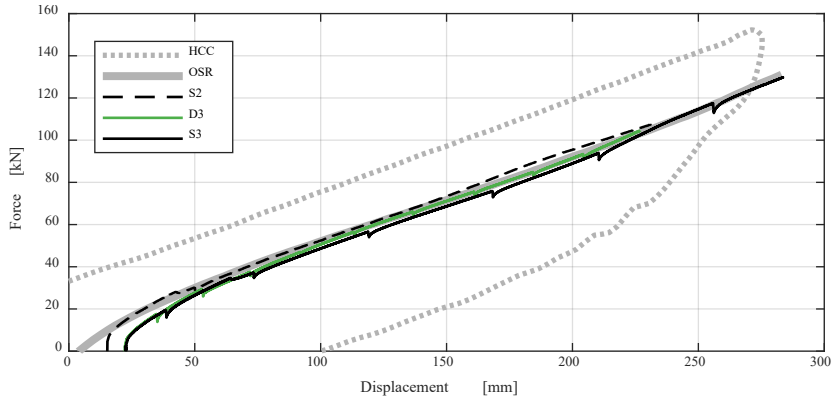

Figure 10: Comparison between control tests on the HDRBs (HCC and OSR) and the load ramp of the tests S2, D3 and S3 (depurated from the friction force and scaled to a single isolator).

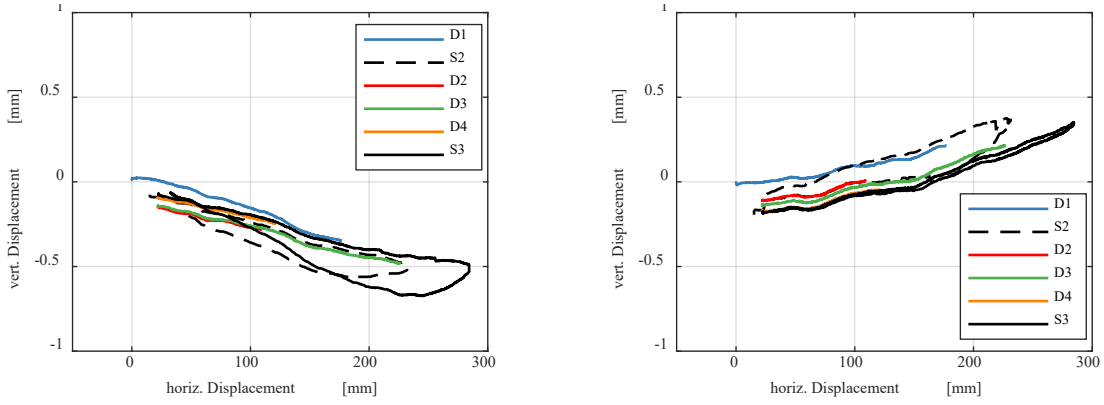

(a) (b)

Figure 11: Comparison between horizontal and vertical displacements recorded by: (a) V2 (HDRB) and T1; (b) V1 (FSB) and T1.

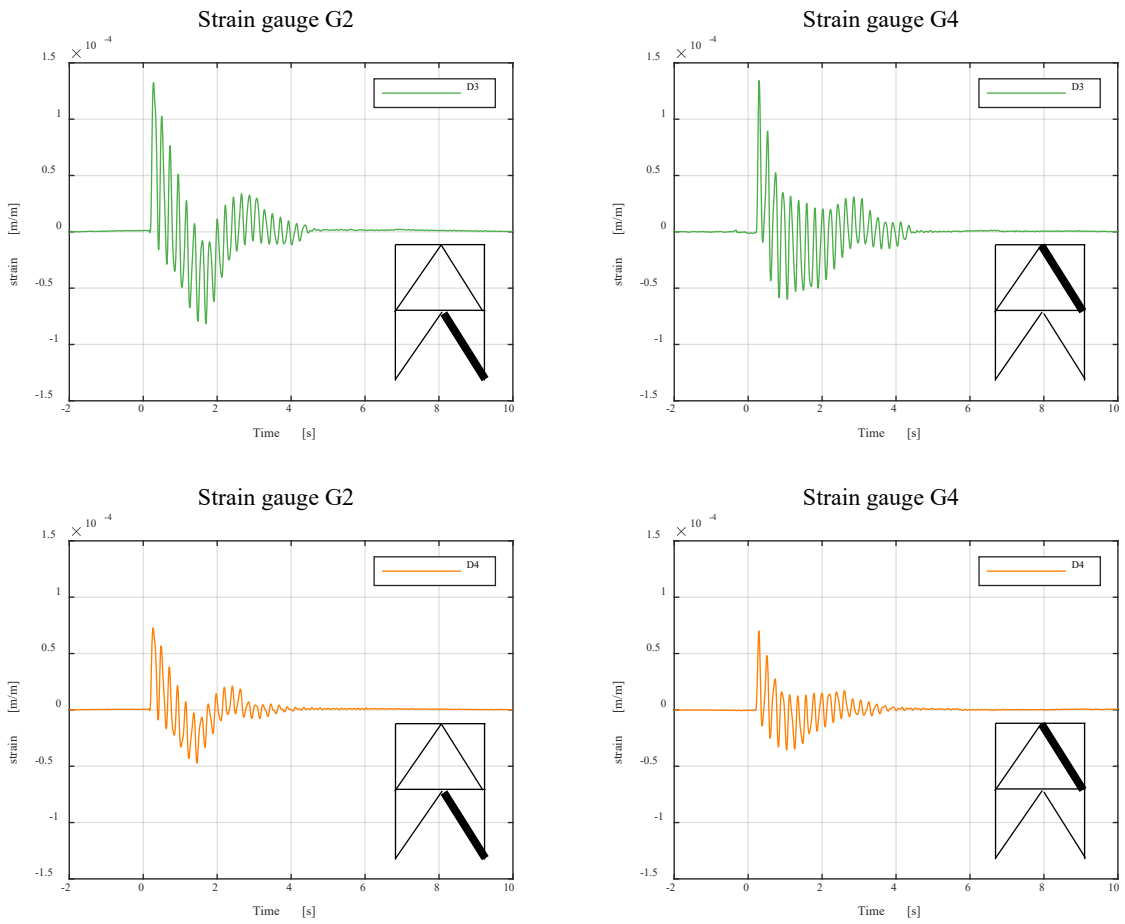

Figure 12: Brace strain time-histories in dynamic tests D3 and D4 (close-up of the release phase).

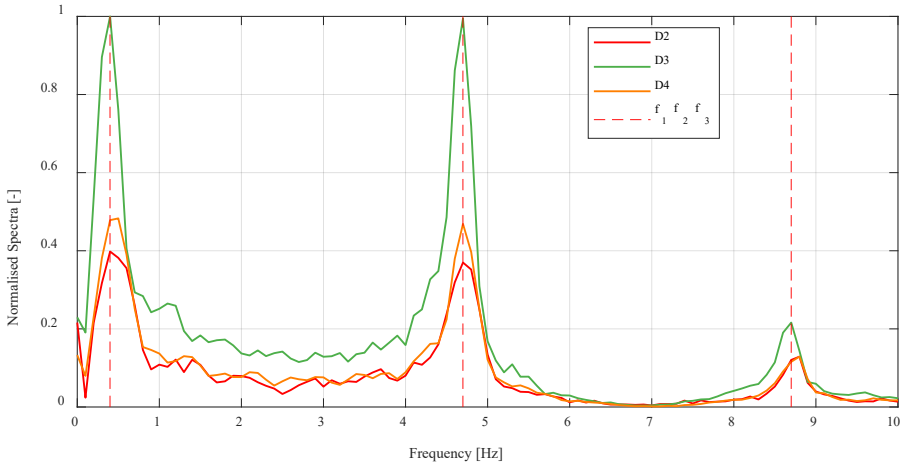

Figure 13: Normalised spectra in dynamic tests D2, D3 and D4 (strain gauges).

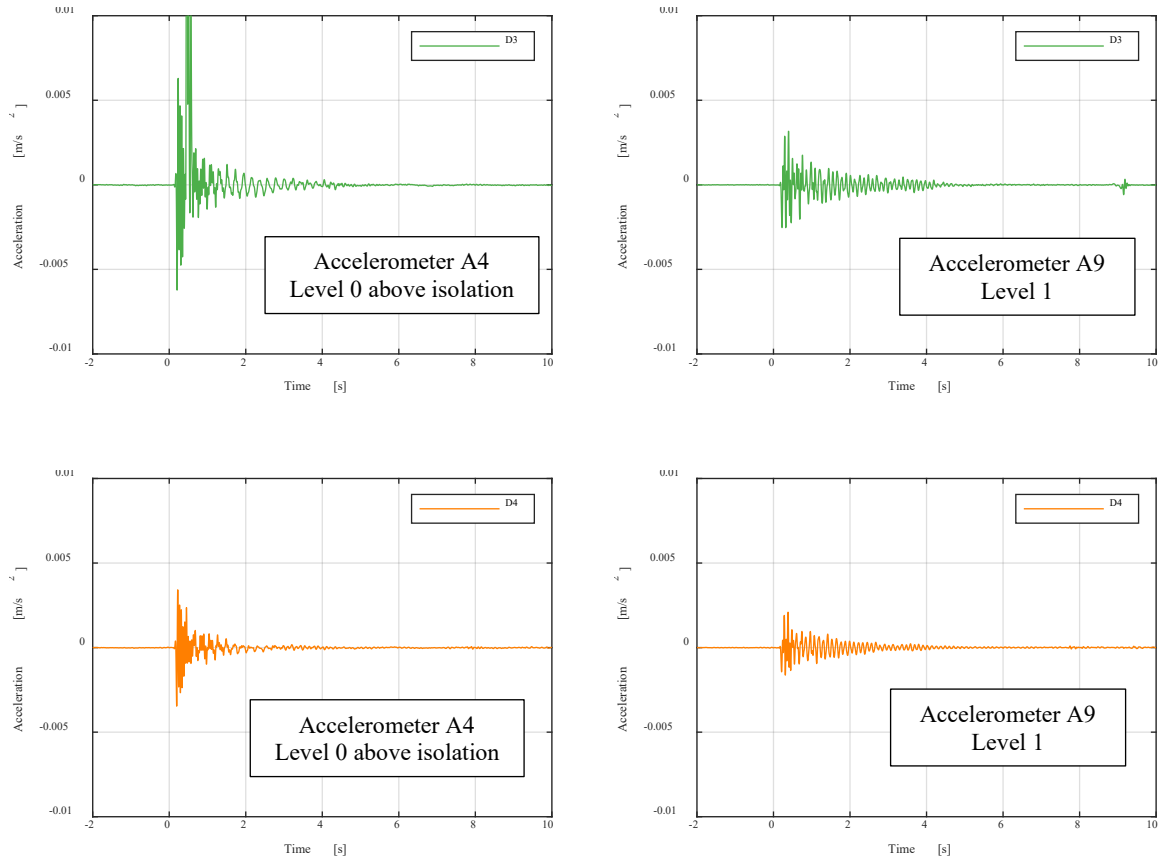

Figure 14: Acceleration time-histories in dynamic tests D3 and D4 (close-up of the release phase).

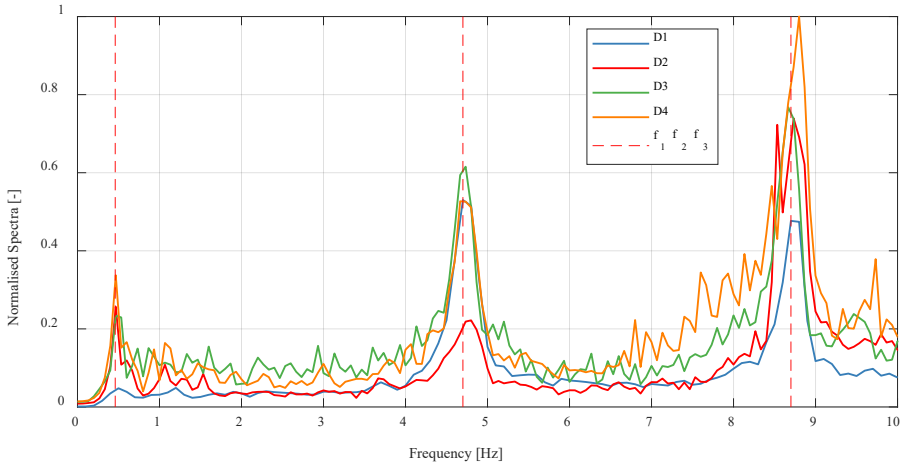

Figure 15: Normalised spectra in dynamic tests D1, D2, D3 and D4 (all the accelerometers).

Push-and-release tests of a steel building with hybrid base isolation

Andrea Dall'Asta[1], Graziano Leoni[1], Laura Gioiella[1], Fabio Micozzi[1], Laura Ragni[2], Michele Morici[1,*], Fabrizio Scozzese[1], Alessandro Zona[1]

[1] School of Architecture and Design, University of Camerino, Italy

[2] Department of Civil and Building Engineering and Architecture, Università Politecnica delle Marche, Italy

*Corresponding Author: michele.morici@unicam.it

Research highlights:

- Experimental testing of a base-isolated building up to displacements not achieved before.
- Push-and-release device integrated in the building for test repetitions during its service life.
- Repeated quasi-static tests with slow loading and unloading.
- Repeated dynamic tests with slow loading and subsequent sudden release.
- Comprehensive recordings of displacements, forces, strains, and accelerations.